Polarimetric Radar Observations and Interpretation of Co-Cross-Polar Correlation Coefficients

ALEXANDER V. RYZHKOV

Cooperative Institute for Mesoscale Meteorological Studies, University of Oklahoma, Norman, Oklahoma

DUSAN S. ZRNIC

National Severe Storms Laboratory, Norman, Oklahoma

JOHN C. HUBBERT AND V. N. BRINGI

Colorado State University, Fort Collins, Colorado

J. VIVEKANANDAN AND EDWARD A. BRANDES

National Center for Atmospheric Research, Boulder, Colorado

(Manuscript received 14 March 2001, in final form 28 August 2001)

ABSTRACT

Preliminary analysis of all components of the polarimetric radar covariance matrix for precipitation measured with the NCAR S-band dual-polarization Doppler radar (S-Pol) and the Colorado State University–University of Chicago–Illinois State Water Survey (CSU–CHILL) radars is presented. Radar reflectivity at horizontal polarization Z_h, differential reflectivity Z_{DR}, linear depolarization ratio LDR, specific differential phase K_{DP}, cross-correlation coefficient $|\rho_{hv}|$, and two co-cross-polar correlation coefficients, ρ_{xh} and ρ_{xv}, have been measured and examined for two rain events: the 14 August 1998 case in Florida and the 8 August 1998 case in Colorado.

Examination of the coefficients ρ_{xh} and ρ_{xv} is the major focus of the study. It is shown that hydrometeors with different types of orientation can be better delineated if the coefficients ρ_{xh} and ρ_{xv} are used. Rough estimates of the raindrop mean canting angles and the rms width of the canting angle distribution are obtained from the co-cross-polar correlation coefficients in combination with other polarimetric variables.

Analysis of the two cases indicates that the raindrop net canting angles averaged over the propagation paths near the ground in typical convective cells do not exceed 2.5°. Nonetheless, the mean canting angles in individual radar resolution volumes in rain can be noticeably higher. Although the net canting angle for individual convective cells can deviate by a few degrees from zero, the average over a long propagation path along several cells is close to zero, likely because canting angles in different cells vary in sign.

The rms width of the canting angle distribution in rain is estimated to vary mainly between 5° and 15° with the median value slightly below 10°.

1. Introduction

Modern dual-polarization radars provide a unique capability to measure the fields of all components of the covariance backscattering matrix, including co-cross-polar correlation coefficients. These, for linearly polarized radars, have so far been scantly explored. Furthermore, until very recently, such data were not available from surveillance weather radars. In this paper, we present full polarimetric data examples obtained with the National Center for Atmospheric Research (NCAR) S-band dual-polarization Doppler radar (S-Pol) and the Colorado State University–University of Chicago–Illinois State Water Survey (CSU–CHILL) research polarimetric radars.

Both radars are linearly polarized and operate at wavelengths of about 10 cm [see Lutz et al. (1997) and Brunkow et al. (2000) for details]. The radars have two receivers that allow simultaneous measurement of copolar and cross-polar components of the backscattered electromagnetic wave. In the ''full polarimetric'' mode of operation, the radars transmit alternately horizontally and vertically polarized waves, and both copolar and cross-polar components of the received waves are recorded. As a result, at least the following nine radar variables can be obtained simultaneously: radar reflectivity factor Z, differential reflectivity Z_{DR}, linear de-

Corresponding author address: Dr. Alexander V. Ryzhkov, CIMMS/NSSL, 1313 Halley Circle, Norman, OK 73069.
E-mail: ryzhkov@nssl.noaa.gov

polarization ratio LDR, total differential phase Φ_{DP} (from which specific differential phase K_{DP} can be derived), cross-correlation coefficient $|\rho_{hv}|$, and the magnitudes and the phases of the two co-cross-polar correlation coefficients: $|\rho_{xh}|$, ($|\rho_{xv}|$), and $\arg(\rho_{xh})$, [$\arg(\rho_{xv})$], respectively. The first five variables have been studied quite well in the literature, whereas the information content of the cross-correlation coefficients ρ_{xh} and ρ_{xv} has not. These need to be examined and are a major focus of this paper. The co-cross-polar correlation coefficients in the circular polarization basis were studied much more extensively. It was established that their magnitudes [ORTT in notations of McCormick and Hendry (1975)] are determined by a degree of common alignment of particles, whereas their phases contain information about the mean canting angle and indicate the presence of non-Rayleigh particles in the radar resolution volume.

Our recent theoretical (Ryzhkov 2001) and observational (Ryzhkov et al. 1999, 2000) studies show that the coefficients ρ_{xh} and ρ_{xv} are determined primarily by characteristics of hydrometeor orientation. Thus, the parameters of the canting angle distribution of the scatterers, such as the mean canting angle and the root-mean-square (rms) width, can be roughly estimated from ρ_{xh} and ρ_{xv} in combination with other polarimetric variables such as Z_{DR} and LDR. Canting angle is defined as an angle between projections of a symmetry axis of spheroidal particle and the vertical onto polarization plane.

It was also shown by Hubbert et al. (1999) and Ryzhkov (2001) that the magnitudes of ρ_{xh} and ρ_{xv} experience pronounced trends with distance if the mean canting angle averaged over a long propagation path (i.e., the ''net'' canting angle) is different from zero. Even a slight canting of a few tenths of a degree can produce a noticeable trend. A similar trend can be caused by antenna feed horn misalignment, nonorthogonality of the ''*H*'' and ''*V*'' waves, cross-coupling between waves with orthogonal polarization, etc. Thus, the $|\rho_{xh,xv}|$ change with distance in relatively uniform precipitation can serve as a quality check for antenna and microwave assembly imperfections and as a tool to validate the simultaneous scheme of transmission/reception that is proposed as an upgrade for the 1988 Doppler Weather Surveillance Radar (WSR-88D). The performance of the simultaneous scheme depends crucially on the net canting angle (Doviak et al. 2000).

Examination of the mean and the rms width of raindrop canting angle distribution estimated with a dual-polarization radar will allow one to assess their possible impact on the accuracy of rainfall measurements. All current polarimetric algorithms for rainfall estimation are based on the models in which raindrops are equioriented such that the axis of rotation is vertical.

In section 2 of this paper, a brief summary of theoretical results regarding physical interpretation of the co-cross-polar correlation coefficients is presented. Section 3 deals with the analysis of the full polarimetric data collected with the NCAR S-Pol in Florida in 1998. A similar dataset obtained with the CSU CHILL radar in Colorado in 1998 is examined in section 4. Discussion and conclusions summarize the results of the study in section 5.

2. Theoretical background

Here we briefly summarize the results obtained in the theoretical paper by Ryzhkov (2001) that addresses the physical interpretation of the co-cross-polar correlation coefficients. These coefficients in the linear ''horizontal–vertical'' polarization basis are

$$\rho_{xh} = \frac{\langle V_{hh}^* V_{hv}\rangle}{\langle |V_{hh}|^2\rangle^{1/2}\langle |V_{hv}|^2\rangle^{1/2}} \quad \text{and} \tag{1}$$

$$\rho_{xv} = \frac{\langle V_{vv}^* V_{hv}\rangle}{\langle |V_{vv}|^2\rangle^{1/2}\langle |V_{hv}|^2\rangle^{1/2}}. \tag{2}$$

In (1) and (2), V_{hh}, V_{vv}, and V_{hv} are the complex voltages corresponding to the two orthogonal copolar and cross-polar components of the radar return, respectively. Brackets mean temporal averaging.

According to Ryzhkov (2001), both co-cross-polar correlation coefficients are directly proportional to $\sin(2\langle\alpha\rangle)$, where $\langle\alpha\rangle$, the mean canting angle in the radar sampling volume, is inversely proportional to the parameter σ, which is the rms width of the canting angle distribution. In rain medium, where $\langle\alpha\rangle$ is small and $|\langle\alpha\rangle| < \sigma$, the following simple formula for $\rho_{xh,xv}$ can be obtained if propagation effects are negligible (Ryzhkov 2001):

$$\rho_{xh,xv} = b_{h,v}\frac{\langle\alpha\rangle}{\sigma}, \tag{3}$$

where the coefficients $b_{h,v}$ depend on drop size distribution. Simulations show that b_h varies mainly within the interval 0.85–0.95, whereas b_v changes from 0.80 to 0.90. Thus, the co-cross-polar correlation coefficients for linear polarizations are determined almost entirely by the parameters $\langle\alpha\rangle$ and σ of the angular distribution of scatterers.

In the absence of propagation effects and for Rayleigh scatterers, the phases of ρ_{xh} and ρ_{xv} are very close to either 0 or $\pm\pi$, depending on the sign of the mean canting angle $\langle\alpha\rangle$ in the radar resolution volume. An additional term in the phase of the co-cross-polar correlation coefficients, the so-called depolarization phase, is present if the scatterers are non-Rayleigh and canted.

The depolarization phase δ_{cr} is potentially a very attractive polarimetric parameter that can be used for detection and sizing of melting hail and for discrimination between wet and dry snow. The phase δ_{cr} is significantly larger than the backscatter differential phase δ_{co}; that is, the argument of the copolar correlation coefficient ρ_{hv}. Another advantage of the depolarization phase is

that it is almost insensitive to the hydrometeor shape and is not affected by particle orientation, whereas δ_{co} tends to zero for quasispherical or randomly oriented scatterers.

The magnitude of the mean canting angle can be obtained from the formula (Ryzhkov 2001)

$$|\langle\alpha\rangle| = 1.87\frac{|\rho_{xh}|(\mathrm{LDR})^{1/2}}{1 - Z_{DR}^{-1}}, \quad (4)$$

and to compute the rms width σ one needs to solve the biquadratic equation

$$\frac{\mathrm{LDR}}{(1 - Z_{DR}^{-1})^2} = 0.05\frac{1 - r^4}{r^2}, \quad (5)$$

where $r = \exp(-2\sigma^2)$. In (4) and (5), the linear depolarization ratio $\mathrm{LDR} = \langle|V_{hv}|^2\rangle/\langle|V_{hh}|^2\rangle$ and differential reflectivity $Z_{DR} = \langle|V_{hh}|^2\rangle/\langle|V_{vv}|^2\rangle$ are expressed in linear units. Both relations imply that the mean canting angle is rather small (less than 10°), the rms width of the canting angle distribution σ is less than about 40°–50°, and Z_{DR} is not very close to 1. Thus, they are applicable for rain medium and, possibly, melting layer. More complex algorithms are required for estimating the parameters of the canting angle distribution in the frozen part of clouds. Both LDR and Z_{DR} should be corrected for differential attenuation before being used in the formula (5). As will be explained later, Eq. (4) is not applicable if depolarization due to propagation occurs.

The magnitudes and phases of the co-cross-polar correlation coefficients are sensitive to propagation effects in precipitation. In the simplest case, if the mean canting angle $\langle\alpha\rangle$ along propagation path is equal to zero, only the phases of ρ_{xh} and ρ_{xv} are affected (Ryzhkov 2001):

$$\rho'_{xh} = \rho_{xh}e^{j\Phi_{DP}/2} \quad (6)$$

$$\rho'_{xv} = \rho_{xv}e^{-j\Phi_{DP}/2}. \quad (7)$$

In (6) and (7), prime superscript denotes measurements in the presence of propagation effects. Note that the difference between the phases of ρ'_{xh} and ρ'_{xv} is very close to the differential phase Φ_{DP} because $\arg(\rho_{xh}) \approx \arg(\rho_{xv})$.

The magnitudes of ρ_{xh} and ρ_{xv} are affected by propagation if the mean canting angle is different from zero; that is, depolarization due to propagation takes place. The theoretical model developed by Ryzhkov (2001) retrieves all polarimetric variables along a propagation path for arbitrary range dependence of the mean canting angle. For example, if we assume that the mean canting angle $\langle\alpha\rangle$ is a random function of range (or propagation differential phase), with modulation that represents a slowly varying net canting angle component θ (Fig. 1a), then the magnitude of ρ_{xh} (or ρ_{xv}) is also modulated in range (Fig. 1b). In the simulations (Fig. 1), we assume that the rms width of the canting angle distribution σ is 10°, rain rate is equal to 30 mm h^{-1} along the propagation path, drop size distribution is Marshall–Palmer,

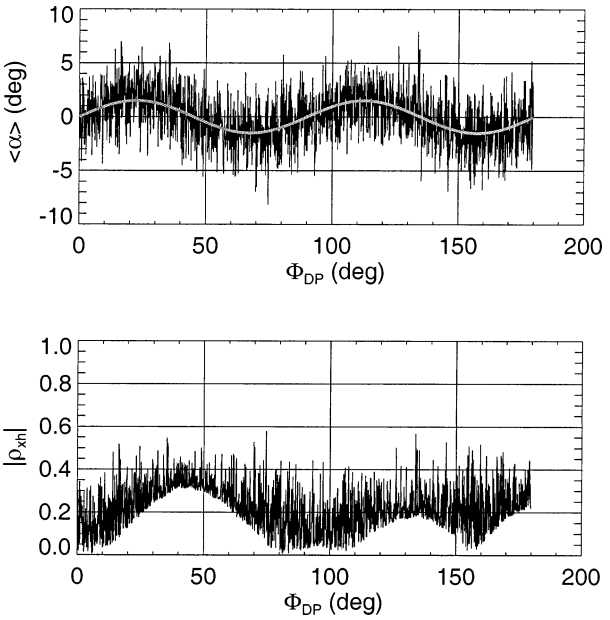

FIG. 1. Theoretical simulation of (top) the mean canting angle $\langle\alpha\rangle$ and (bottom) the corresponding magnitude of the co-cross-polar correlation coefficient $|\rho_{xh}|$ as functions of differential phase Φ_{DP}. The rms width of the canting angle distribution σ is assumed to be 10°.

and raindrop shape is given by Pruppacher and Pitter (1971). In this example, the net component of the canting angle θ (thick gray line in Fig. 1a) slowly oscillates around zero level. If the canting angle has a net positive or negative offset (in other words, if θ or $\langle\alpha\rangle$ averaged over the whole propagation path is different from zero), then the magnitudes of ρ_{xh} and ρ_{xv} are expected to have a positive trend with distance (Hubbert et al. 1999; Ryzhkov 2001). Note that the presence of such a persistent trend in observational data can also be caused by artifacts in a dual-polarization radar (e.g., cross-coupling, misalignment of a feed horn, nonorthogonality of *H* and *V*, etc).

3. Observations with the NCAR S-Pol radar

Weather observations with the NCAR S-Pol radar have been made during the field project named PRECIP98. The S-Pol radar was deployed near Melbourne, Florida, and the radar data were collected during August–September 1998. In the course of the experiment, the ''full polarimetric'' mode of observations was occasionally used. Here, we present the full polarimetric (full pol) data for a strong localized thunderstorm close to the radar that occurred on 14 August 1998. During a relatively short period of observations in the full pol mode, the storm contained two convective cells, the strongest of which was closer to the radar. Next, we will examine multiparameter radar data in the range–height indicator (RHI) cross sections of the storm taken at the azimuths corresponding to the center of the stronger convective cell (hereafter ''convective region'') and to

the periphery of the same cell embedded in a stratiform background (''stratiform region'').

a. Convective region

Multiparameter data fields including Z, Z_{DR}, LDR, K_{DP}, $|\rho_{xh}|$, and $|\rho_{hv}|$ in the vertical cross section are represented in Fig. 2. The data from radar rays spaced 1° in elevation were used to construct the RHI plot. Values of LDR and $|\rho_{hv}|$ along each radial were obtained after averaging over seven successive gates with the spacing of 0.15 km. Thirteen and 25 gates were used for averaging of Z_{DR} and $|\rho_{xh}|$, respectively. Linear fits for differential phase Φ_{DP} were used to estimate K_{DP}. Radial resolution for K_{DP} estimates is about 2 km (13 gates) if radar reflectivity exceeds 40 dBZ and 3.8 km (25 gates) otherwise. Figure 2 reveals the complementary character of multiparameter information. None of the variables duplicates others. Each one provides different information and gives insight regarding cloud and precipitation microphysics.

The convective cell at the range 15–25 km in Fig. 2 has an internal structure suggestive of two merging cores. There are two regions at the periphery of the cell centered at the distances of 18 and 22 km from the radar and marked by two separate streaks of increased Z aloft and separate maxima of radar reflectivity factor exceeding 55 dBZ in the melting layer at the height of about 3.5 km. Two maxima of Z in the melting layer coincide with pronounced K_{DP} maxima well over 2.5° km^{-1}. Both regions are associated with high Z_{DR} values below the freezing level. We can speculate that these regions are associated with updrafts, whereas the area between (centered at about 20 km from the radar) might coincide with a downdraft. This interpretation is consistent with the pattern of Doppler velocities (not shown here), indicating radial convergence at low and midlevels and divergence near the top of the cloud, collocated with the regions of suggested updrafts. The downdraft area is characterized by lower values of Z and Z_{DR} and very intense precipitation near the ground with rain rate $R > 100$ mm h^{-1}. The latter estimate is made using the formula $R(K_{DP}) = 40.6\, K_{DP}^{0.866}$ (Doviak and Zrnic 1993). The maximum K_{DP} value near the ground is about 2.9° km^{-1}.

It is likely that, within the downdraft region, rain near the ground is characterized by relatively small median drop diameters (inferred from a small Z_{DR}) but very high drop concentration. It is probably mixed with moderate-size graupel or even small hail at higher altitudes, as can be concluded from low values of Z_{DR} and moderate values of Z and K_{DP}. Within the updraft areas, raindrops are bigger, and their total concentration is lower than in the downdraft region. Three-dimensional wind field information is needed to make a more reliable interpretation of the observed polarimetric signatures.

The upward extension of the K_{DP} and Z_{DR} columns to 7 km aloft within the stronger, closer to the radar, updraft indicates the presence of supercooled liquid drops above the freezing level (Hubbert et al. 1998). At the top of the columns (at the range 19 km and height 7 km), a local increase of linear depolarization ratio (''LDR cap''), usually associated with rapidly freezing raindrops (Jameson et al. 1996), is evident.

The LDR field exhibits a slightly bent, vertically oriented region of lower values (shown in green in Fig. 2) in the center of the convective core. This region contrasts the surrounding environment by its relatively low values of LDR (below −24 dB). This LDR signature is an indication of quasispherical scatterers, most likely small or moderate-size graupel that produces the rain below. Larger, hail-size frozen hydrometeors usually cause larger LDR (> −20 dB). The observed LDR signature is consistent with the type of rain below in the downdraft region (small drops in high concentration) that very often originates from melting of small or moderate-size graupel (Ryzhkov and Zrnic 1996b). This LDR signature is also consistent with the Z_{DR} values close to zero and relatively high values of the cross-correlation coefficient $|\rho_{hv}|$ above 6 km, both of which point to the quasispherical nature of hydrometeors. Considerably higher values of LDR (and correspondingly higher Z_{DR} and lower ρ_{hv}) are seen at the periphery of the convective core above the freezing level. These could be attributed to aggregated snowflakes with highly irregular shapes that are possibly mixed with graupel.

The most fascinating of the data are the co-cross-polar correlation coefficients ρ_{xh} and ρ_{xv}; interpretation and analysis of these follows. The field of $|\rho_{xh}|$ averaged over 25 consecutive range gates (3.8 km) along each radial is shown in the bottom central panel of Fig. 2. The magnitude of ρ_{xh} exhibits well-defined spatial structure with the lowest values of $|\rho_{xh}|$ within the melting layer outside the convective cell, and the highest values observed in some regions of low reflectivity aloft within the altitude interval 8–12 km. Below the melting level, $|\rho_{xh}|$ is lower in convective rain than in stratiform rain.

The observed spatial structure of the magnitude of the co-cross-polar correlation coefficient can be interpreted in terms of particle orientation using the theoretical model developed by Ryzhkov (2001). As mentioned in section 2, $|\rho_{xh}|$ is directly proportional to $|\sin(2\langle\alpha\rangle)|$, where $\langle\alpha\rangle$ is the mean canting angle in the radar sampling volume, and is inversely proportional to the parameter σ, which is the rms width of the canting angle distribution. In the melting layer, where melting snowflakes are wobbling, σ is always large, and $|\rho_{xh}|$ drops, regardless of the mean canting angle. Near cloud tops, small crystals can be well aligned along the direction of the electric field within thunderstorms if the field is strong enough. These crystals might exhibit a high degree of common alignment (and, thus, small σ) and could have quite large mean canting angles, depending on the orientation of the electric field vector. Therefore, large values of $|\rho_{xh}|$ are expected in these zones.

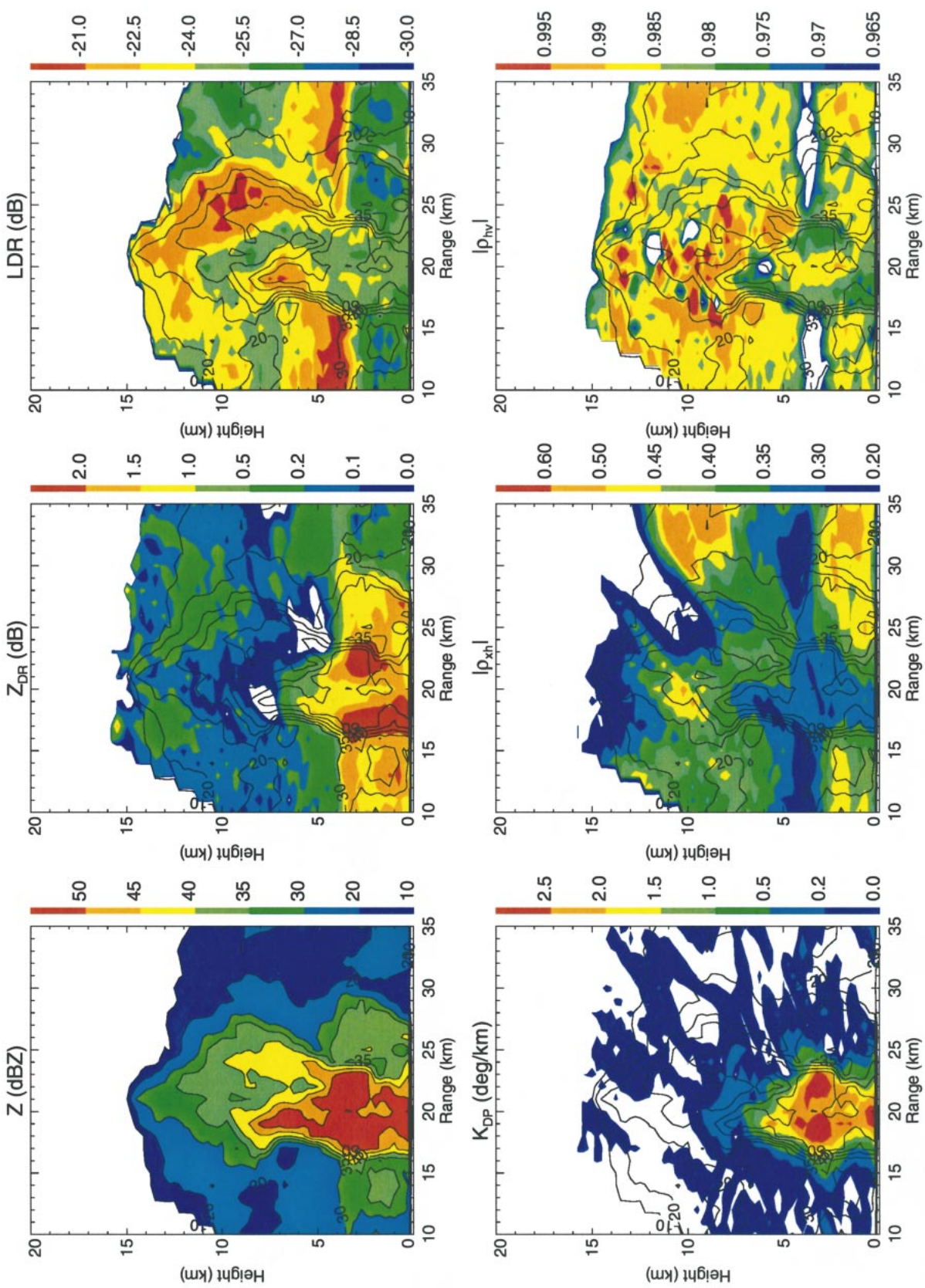

FIG. 2. Composite plot of Z, Z_{DR}, LDR, K_{DP}, $|\rho_{xh}|$, and $|\rho_{hv}|$ in the RHI cross section of the storm on 14 Aug 1998 in Florida. Superimposed on the plots are contours of Z. The azimuth angle is 168.5°.

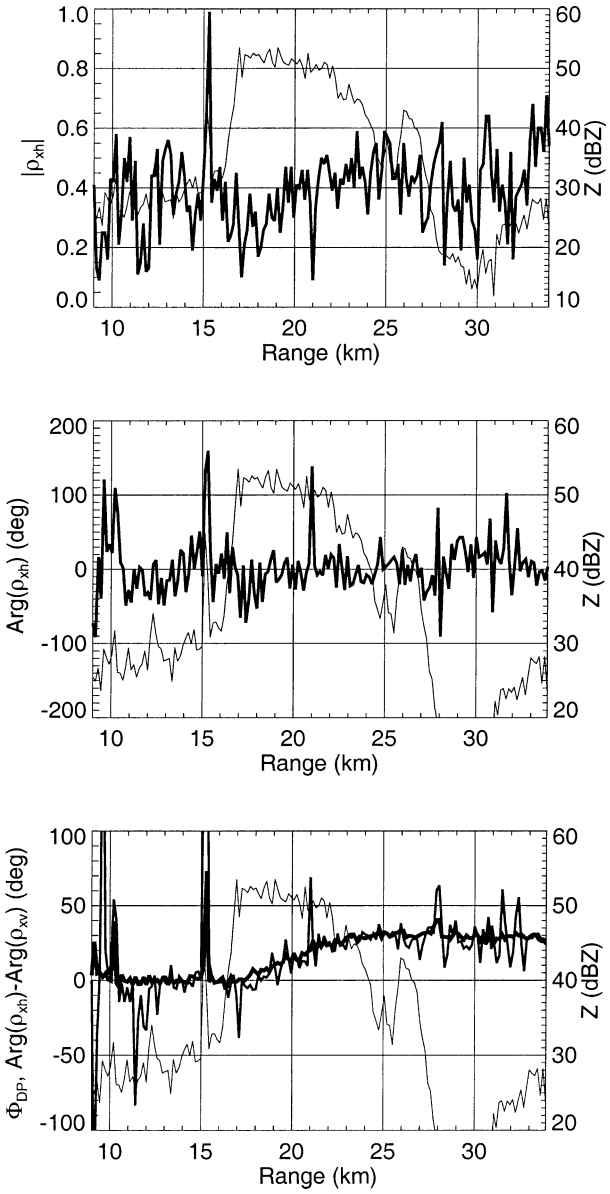

FIG. 3. Radial dependencies of nonfiltered (top) $|\rho_{xh}|$, (middle) $\arg(\rho_{xh})$, and (bottom) $\arg(\rho_{xh}) - \arg(\rho_{xv})$ and Φ_{DP} (heaviest curve) for the case of 14 Aug 1998 (shown by thick lines). Radial dependence of Z (thin lines) is plotted in all three panels. Az = 168.5°; El = 0.6°.

Figure 3 illustrates raw ρ_{xh} data (without any averaging) in rain along the radar beam at the elevation angle of 0.6° for the azimuthal direction corresponding to the RHI cross section presented in Fig. 2. As can be seen (Fig. 3a), the magnitude of $|\rho_{xh}|$ varies mainly between 0.3 and 0.5 in rain. A positive trend in the $|\rho_{xh}|$ data is visible within the core of intense rain between 17 and 25 km, where the differential phase Φ_{DP} increases by more than 30° (Fig. 3c). This trend is most likely an indication of propagation effect in a medium of canted drops that have a net (average) canting angle θ slightly different from zero within the range interval 17–25 km. This is in accord with Ryzhkov (2001), who predicts that the increase of $|\rho_{xh}|$ (i.e., $\Delta|\rho_{xh}|$) caused by propagation is roughly proportional to the product $|\sin 2\theta|\,\Delta\Phi_{DP}$, where $\Delta\Phi_{DP}$ is the differential phase increment within the examined range interval. In this particular case, we have found that $|\theta| \approx 1°$ yields a good match between the theoretical simulation and results of observations. Here, we stress that $\langle\alpha\rangle$ is the mean canting angle in the radar sampling volume, varying from gate to gate, and θ is its net value obtained by averaging $\langle\alpha\rangle$ over a few kilometers in range (Fig. 1).

Analysis of the other co-cross-polar correlation coefficient, ρ_{xv}, shows that it correlates very well with ρ_{xh} in both magnitude and phase. It was found that the magnitude of ρ_{xv} is slightly biased due to radar data processing error that has been discovered only after the measurements were made. This error, however, does not affect the phase of ρ_{xv}.

Radial dependence of the phase of ρ_{xh} is illustrated in Fig. 3b, and the difference between the phases of ρ_{xh} and ρ_{xv} as a function of range from the radar is shown in Fig. 3c. Although both phases $\arg(\rho_{xh})$ and $\arg(\rho_{xv})$ fluctuate intensely, their difference is quite smooth and follows Φ_{DP} very well, as predicted by theory (Hubbert et al. 1999; Ryzhkov 2001). Thus, in principle, the differential phase Φ_{DP} can be estimated from the phase difference between ρ_{xh} and ρ_{xv}.

The measured phase of the co-cross-polar correlation coefficient exhibits behavior that is somewhat unexpected. Indeed, the theory predicts very deep oscillations of this phase in rain (within the $-\pi$ to π interval) due to rapid spatial changes of the sign of the mean canting angle $\langle\alpha\rangle$ along the radar beam if the net canting angle θ is close to zero. In fact, smaller fluctuations about the system phase value are evident in Fig. 3b. This can be attributed to the lack of polarization isolation between two orthogonal channels, that is, to the coupling between the channel receiving the strong copolar component of the radar signal and the channel where the much weaker cross-polar component is received. This coupling was actually confirmed in the current S-Pol radar. Unwanted coupling between orthogonal channels affects primarily depolarization variables such as ρ_{xh}, ρ_{xv}, and LDR. It can be shown that LDR, $|\rho_{xh}|$, and $|\rho_{xv}|$ become positively biased in the presence of coupling. The biases are larger in the areas with low intrinsic LDRs, such as rain. Interestingly, despite the fact that both $\arg(\rho_{xh})$ and $\arg(\rho_{xv})$ are compromised by the interchannel coupling, their difference is robust and agrees well with Φ_{DP}, in full accord with theory (Fig. 3c).

b. Stratiform region

A vertical cross section of the radar variables taken at the periphery of the storm exhibits mostly a stratiform type of precipitation with well-pronounced melting lay-

er signatures in the Z_{DR}, LDR, $|\rho_{xh}|$, and $|\rho_{hv}|$ fields (Fig. 4). Note that the ''bright band'' signature is absent in the radar reflectivity field. The regions of light-to-moderate rain below the melting layer and dry aggregated snow above the melting layer are well contrasted in the Z_{DR}, LDR, and $|\rho_{xh}|$ fields. The contrast is sharpest in the Z_{DR} and LDR fields. Linear depolarization ratio has, probably, stronger discriminatory power if rain is light, for which differential reflectivity does not differ much from that for dry snow with approximately the same radar reflectivity factor (Ryzhkov and Zrnic 1998). The cross-correlation coefficient $|\rho_{hv}|$ usually helps detect melting snow and large hail (in this respect, it can serve as a proxy for LDR) but definitely lacks LDR's capability to discriminate between rain and dry snow and to reveal certain coherent structures aloft associated with small graupel/supercooled drops seen in Fig. 2 and discussed earlier.

The most striking and interesting signature in Fig. 4 is the area of very high $|\rho_{xh}|$ near the cloud top, where Z is between 10 and 20 dBZ. Radial dependencies of the magnitude and phase of the co-cross-polar correlation coefficient ρ_{xh} for the ray intersecting this area are shown in Fig. 5. The increase of $|\rho_{xh}|$ is accompanied by relatively ''flat'' arg(ρ_{xh}) and a decrease of total differential phase Φ_{DP} with range. These signatures are most likely caused by well-aligned crystals with the orientation substantially different from either vertical or horizontal. The negative slope of Φ_{DP} (or negative K_{DP}) is evidence of the fact that horizontal projection on the plane of polarization of those scatterers is smaller than their vertical projection. This negative K_{DP} signature is usually associated with positive values of differential reflectivity Z_{DR} that is heavily weighted by larger scatterers such as aggregates. Analysis of other cases indicates that K_{DP} can be either positive or negative in the regions of high $|\rho_{xh}|$, depending on the ratio of horizontal and vertical projections of crystals. Weak oscillations of arg(ρ_{xh}) point to a large mean canting angle $\langle\alpha\rangle$ and a relatively small width of the canting angle distribution σ; thus, the sign of the mean canting angle remains the same through the region. As was shown in previous studies (Caylor and Chandrasekar 1996; Krehbiel et al. 1996, among others), unusual crystal orientation is caused by strong electric fields. Therefore, measuring the co-cross-polar correlation coefficients in the linear polarization basis can be helpful in identifying electrically charged zones within clouds.

c. *Estimation of the width of the canting angle distribution*

Equation (5) was used to estimate the rms width of the canting angle distribution in the rain medium below the melting layer. As was already stated, the estimates of the co-cross-polar correlation coefficients and depolarization ratio obtained with the S-Pol radar are likely biased in rain due to coupling between two orthogonal channels. One of the possible reasons for coupling is a slight nonorthogonality of the two basic linear polarizations; this was discovered after the fact with more precise antenna pattern measurements. Rough correction of LDR based on the measured degree of nonorthogonality can be made using the formula

$$\mathrm{LDR}' = \mathrm{LDR} - \Delta\mathrm{LDR}, \tag{8}$$

where LDR is the measured linear depolarization ratio, LDR′ is the corrected (intrinsic) value, and ΔLDR (dB) $= -29.6$ dB. All variables in (8) are expressed in linear (not logarithmic) units. Measured and corrected values of LDR differ by less than 1 dB if LDR′ > -24 dB. The difference can be as high as 3 dB if LDR′ $= -30$ dB.

We took two subsets of the data presented in Figs. 2 and 4 and computed σ at altitudes below 5 km. Figure 6 represents the fields of Z, Z_{DR}, LDR, and σ in the region containing the strong convective cell. Within the convective cell in the center of the plot, the rms width of the canting angle distribution is larger than at its periphery. The rms width σ exceeds 15° in the center of the cell at heights above 1 km. It drops to smaller values (between 5° and 10°) at the periphery of the cell. A similar cross section for a stratiform part of the storm is shown in Fig. 7. Within the first kilometer above the ground, the average σ is slightly less than 10°. Both Figs. 6 and 7 reveal a steady increase of σ with height that is expected. Raindrops originating from either melting snowflakes, graupel, or hailstones usually stabilize their orientation on the way to the ground, thus reducing σ. Some increase of σ is possible in the surface layer (within 100 m above the ground) due to stronger wind shear that usually occurs in the near proximity of the surface. However, this effect would be difficult to resolve with a radar beam pointing at a nonzero elevation angle and having a width of 1°. We believe that the algorithm gives us reliable estimates of σ even in the melting layer where Z_{DR} is high. The method fails above the melting layer because Z_{DR} approaches 0 dB, and the ratio LDR/$(1 - Z_{DR}^{-1})^{1/2}$ becomes unstable.

Analyzing histograms of σ within the lowest kilometer above the ground, we conclude that σ generally varies between 5° and 15°, with its median value slightly less than 10°. Note that Olsen (1981) quotes values of σ in rain that are two times higher (obtained from depolarization measurements on terrestrial links). This could be due to the fact that most terrestrial communication links have propagation paths in the close vicinity of the ground, where airflow is more disturbed by the surface. On the other hand, our estimated values of σ are substantially higher than those predicted by theory (Beard and Jameson 1983) and reported by McCormick and Hendry (1974)—less than 4°.

Our findings have implications for polarimetric rainfall estimation based on K_{DP}, which is proportional to the factor $r = \exp(-2\sigma^2)$. The σ values between 10° and 15° lead to a K_{DP} decrease of 6%–13% that has to

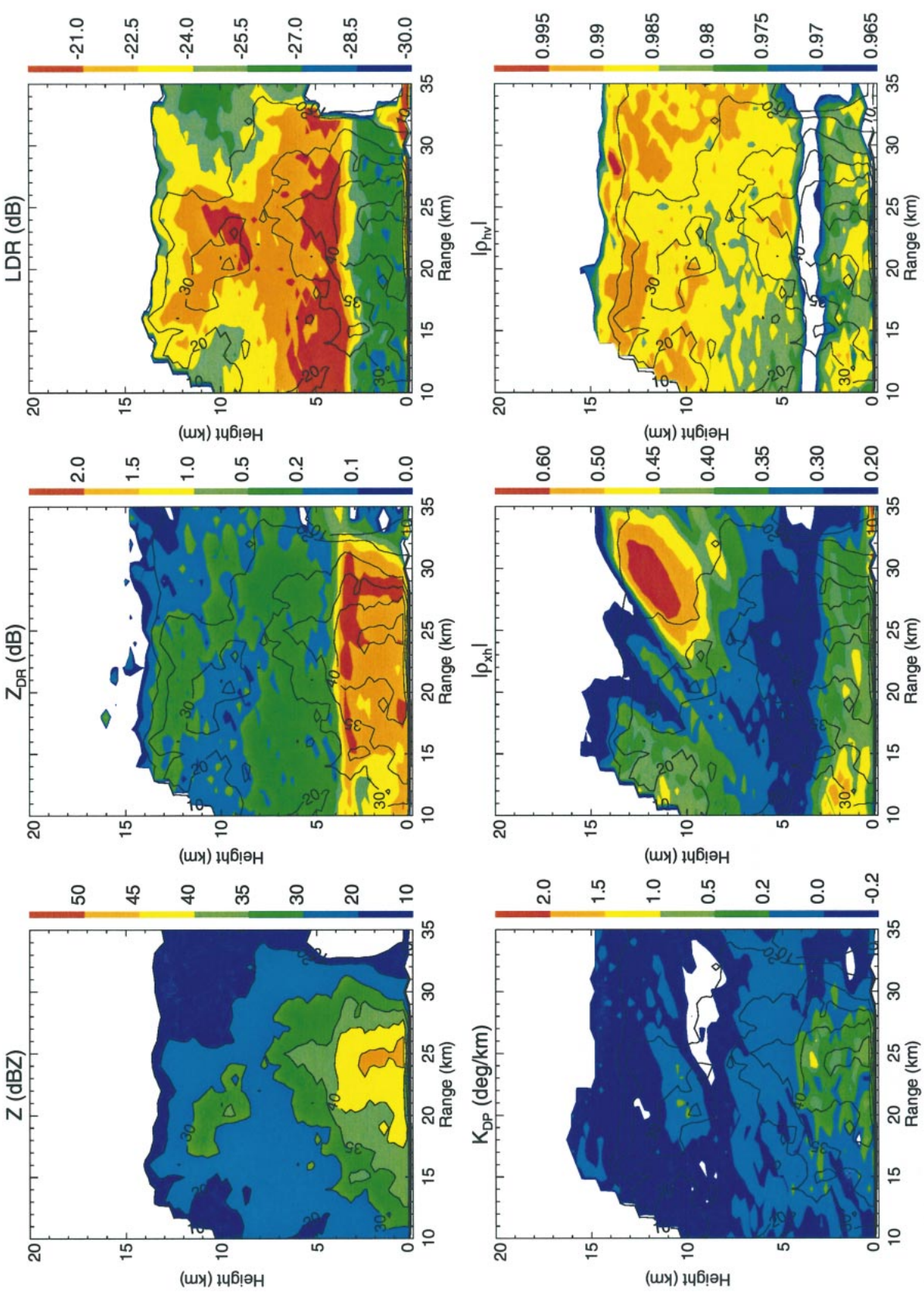

FIG. 4. Same as in Fig. 2, but for the azimuth of 189.0°.

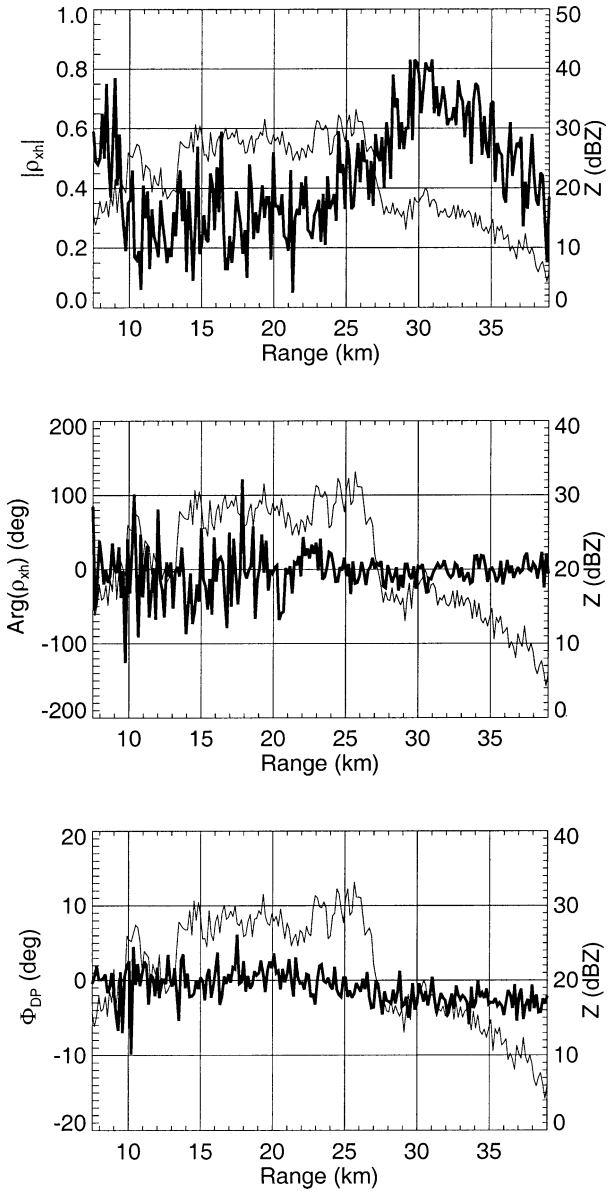

FIG. 5. Radial dependencies of nonfiltered (top) $|\rho_{xh}|$, (middle) $\arg(\rho_{xh})$, and (bottom) Φ_{DP} for the case of 14 Aug 1998 (shown by thick lines). Radial dependence of Z (thin lines) is plotted in all three panels. Az = 189.0°; El = 21.3°.

be taken into account. This fact alone can explain the negative bias of about 10% in polarimetric rainfall estimates involving K_{DP} that was reported by Ryzhkov and Zrnic (1996a) and Brandes et al. (2001).

We are not able to estimate the magnitude of the mean canting angle $|\langle\alpha\rangle|$ using formula (4) for the S-Pol data because the measured values of $|\rho_{xh}|$ (as well as LDR) are positively biased due to the system errors mentioned in section 3a. Rough correction of LDR via (8) seems reasonable. Nonetheless, there is no simple way to make a similar correction of $|\rho_{xh}|$. Our understanding is that, although the measured magnitudes of ρ_{xh} are positively biased, their relative change throughout the storm is fairly robust and can be used for hydrometeor classification and estimation of the net canting angle θ. Theoretical simulations indicate that the estimate of θ is more sensitive to radial gradients of $|\rho_{xh}|$ than to its absolute value.

4. Observations with the CSU–CHILL polarimetric radar

It is instructive to compare the results of observations conducted in Florida with similar full polarimetric multiparameter data obtained with another polarimetric radar, in another geographical region, and from another type of storm. Here we present data collected with the CSU–CHILL radar from a Colorado hail-bearing storm observed on 8 August 1998.

a. Multiparameter data

This storm had a high-reflectivity core with $Z > 54$ dBZ confined within the range 32–34 km from the radar and within the lowest 3-km height interval (Fig. 8). This core is apparently associated with a mixture of rain and melting hail. Supporting indications are 1) high Z (up to 57 dBZ), 2) a well-pronounced protrusion in the Z_{DR} field characterized by a low Z_{DR} area descending 1–1.5 km below the freezing level, and 3) relatively high values of LDR (> -26 dB) at the top of the high-reflectivity core. The hail, however, is not very large and, as suggested by high values of Z_{DR} at low levels, very likely melts on the way to ground.

The magnitude of the co-cross-polar correlation coefficient ρ_{xh} has a pattern that is quite uniform in the vertical direction and shows a gradual increase with range. Vertical uniformity of $|\rho_{xh}|$ is consistent with the observation in the convective cell of the Florida storm. The positive trend of $|\rho_{xh}|$ is an indication of nonzero net canting angle. This trend is clearly seen in Fig. 9, where radial dependencies of $|\rho_{xh}|$, $|\rho_{xv}|$, $\arg(\rho_{xh})$, $\arg(\rho_{xv})$, and $\arg(\rho_{xh}) - \arg(\rho_{xv})$ are plotted along with Z and Φ_{DP} for the ray at the elevation angle of 1.7°. Comparison with the model simulations described in Ryzhkov (2001) gives an estimate of the net canting angle θ somewhere between 2.0° and 2.5° for this particular radial. We also estimated θ for the radial corresponding to 3.5° elevation (not shown) and obtained a value of θ approximately two times smaller.

Reliable measurements of the other co-cross-correlation coefficient, ρ_{xv}, are available from the CHILL radar and can be compared with the ones for ρ_{xh}. Figs. 9a and 9b show very good correlation between ρ_{xh} and ρ_{xv}, in both magnitudes and phases. The phases of ρ_{xh} and ρ_{xv} exhibit very deep fluctuations due to changes in the sign of the mean canting angle in much better agreement with theory than similar data from Florida (Figs. 3 and 5). This we attribute to the better polarization isolation between orthogonal channels on the

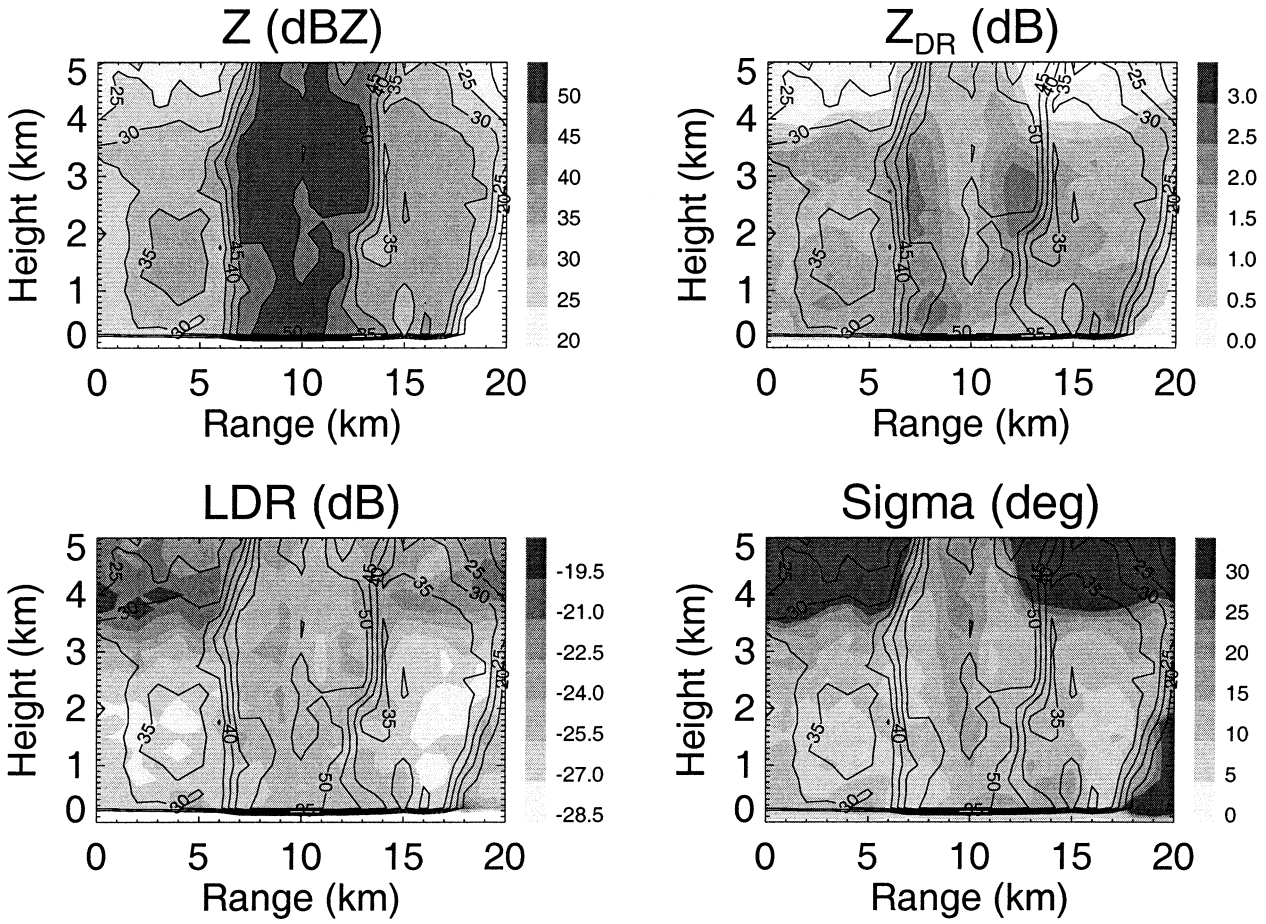

FIG. 6. Composite RHI plot of Z, Z_{DR}, LDR, and σ (the rms width of the canting angle distribution) for the storm on 14 Aug 1998 in Florida. Az = 168.5°.

CHILL radar. Note also the lower values of LDR in the CHILL data in light-to-moderate rain and noticeably lower levels of $|\rho_{xh}|$ and $|\rho_{xv}|$ observed in the Colorado storm. The magnitudes of ρ_{xh} in rain measured by the S-Pol radar vary mainly between 0.3 and 0.5, whereas the corresponding values of $|\rho_{xh}|$ estimated with the CHILL radar are between 0.1 and 0.3.

As in the Florida case, the difference in the arguments of ρ_{xh} and ρ_{xv} shows the same trends as Φ_{DP} (Fig. 9c). Nonetheless, this correspondence is not as obvious as in the Florida case (Fig. 3c) because differential phase increases only about 10° along the propagation path through precipitation in the Colorado storm.

b. Estimation of the parameters of raindrop orientations

Because the estimates of $|\rho_{xh}|$ and $|\rho_{xv}|$ made with the CHILL radar are less biased, and differential phase span through the Colorado storm is relatively small, we have confidence in the derived magnitudes of the mean canting angle $\langle\alpha\rangle$ from relation (4). There is also no need to correct the measured linear depolarization ratio in order to estimate the rms width of the canting angle distribution σ. Relation (5) was used to compute the parameter σ . The fields of the σ and $|\langle\alpha\rangle|$ estimates are presented in Fig. 10.

Figure 10a shows that the rms width σ varies mainly between 6° and 9° in a rain region below the freezing level. These values are slightly smaller than the ones estimated for the Florida storm. Similarity between the σ and Z_{DR} fields (see Fig. 8b) is somewhat suspicious and might be a result of either uniformity of the LDR field or some deficiency of the method. Note that in the Florida case there is no such a strong correlation between σ and Z_{DR}. Unrealistically high values of σ at the periphery of the precipitation area are related to a positive bias in the LDR estimates caused by low signal-to-noise ratio. As was stated earlier, the algorithm (5) is not applicable to the frozen part of the storm where differential reflectivity is close to 0 dB. Thus, the estimates of σ in the frozen region above the melting level illustrated in Fig. 10a are meaningless.

Figure 10b. represents the magnitude of the mean canting angle derived from the relation (4) in the vertical cross-section of the storm. Again, the estimates of $|\langle\alpha\rangle|$

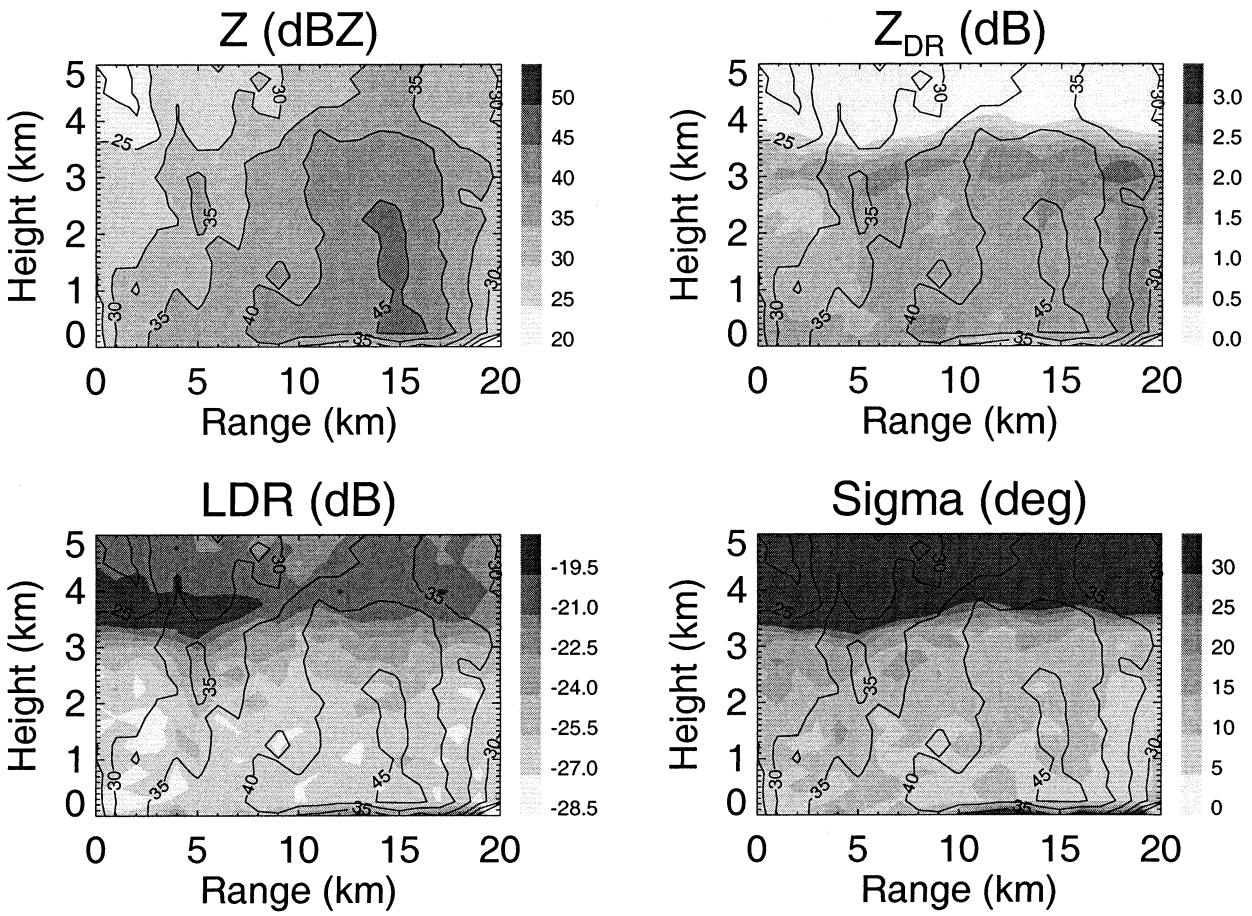

FIG. 7. Same as in Fig. 6, but for Az = 189.0°.

outside the rain area are not trustworthy because LDR is biased by low signal-to-noise ratio, or Z_{DR} is very close to zero. Within the area of larger SNR, the magnitude of the mean canting angle does not exceed 4°, with the average value of about 2°.

5. Discussion and summary

Analysis of all components of the polarimetric radar covariance matrix and their derivatives measured by dual-polarization radars demonstrates a great potential of multiparameter measurements for hydrometeor identification, quantification of precipitation amounts, and calibration of dual-polarization radars. Even the co-cross-polar correlation coefficients measured in the linear ''horizontal–vertical'' polarization basis, which for a long time were considered insignificant, are a source of useful information. Here we will discuss some practical issues regarding possible use of these coefficients.

1) The magnitudes of the co-cross-polar correlation coefficients ρ_{xh} and ρ_{xv} have pronounced signatures in the regions of vertically aligned crystals with orientations determined by the direction of the electric field vector. Therefore, anomalously high values of $|\rho_{xh}|$ or $|\rho_{xv}|$, exceeding 0.5–0.6 (often combined with negative K_{DP}), could indicate electrically charged zones in the clouds. The melting layer can also be detected by lower values of $|\rho_{xh}|$ ($|\rho_{xv}|$), but alternate polarimetric variables, LDR and $|\rho_{hv}|$, for example, have more discernible signatures in the melting layer.

2) The zones of tilted crystals are marked by very ''plain'' behavior of the arg(ρ_{xh}) and arg(ρ_{xv}), that is, by the absence of deep spatial fluctuations, caused by the changes in the sign of the mean canting angle. In this sense, the phases of ρ_{xh} and ρ_{xv} can also be used to recognize electrically active zones. The very noisy and oscillatory character of arg(ρ_{xh}) and arg(ρ_{xv}) likely will hinder identification of non-Rayleigh scatterers such as large hail or large wet snowflakes, postulated by Ryzhkov (2001). This matter requires more scrutiny. Perhaps the use of the co-cross-correlation coefficients measured in the circular polarization basis would be a more feasible option for detecting large non-Rayleigh particles and gauging their size.

3) The difference arg(ρ_{xh}) − arg(ρ_{xv}) yields an approximation for the total differential phase Φ_{DP}, although it is noisier than the Φ_{DP} estimate obtained as the phase of ρ_{hv}. In principle, this alternate estimate of

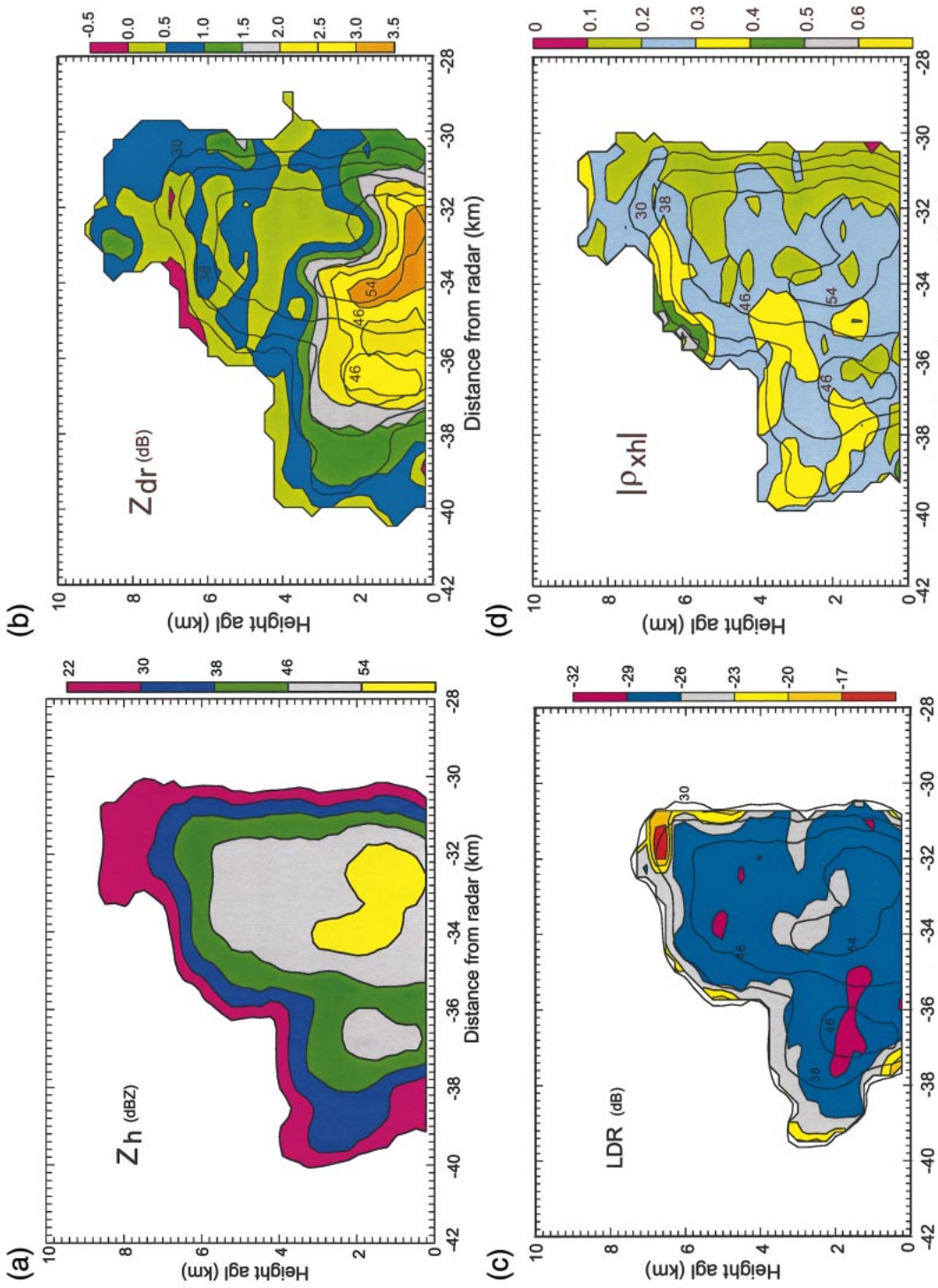

FIG. 8. Composite plot of (a) Z_h, (b) Z_{DR}, (c) LDR, and (d) $|\rho_{xh}|$ in the RHI cross section of the storm on 8 Aug 1998 in Colorado. Superimposed on the plots are contours of Z.

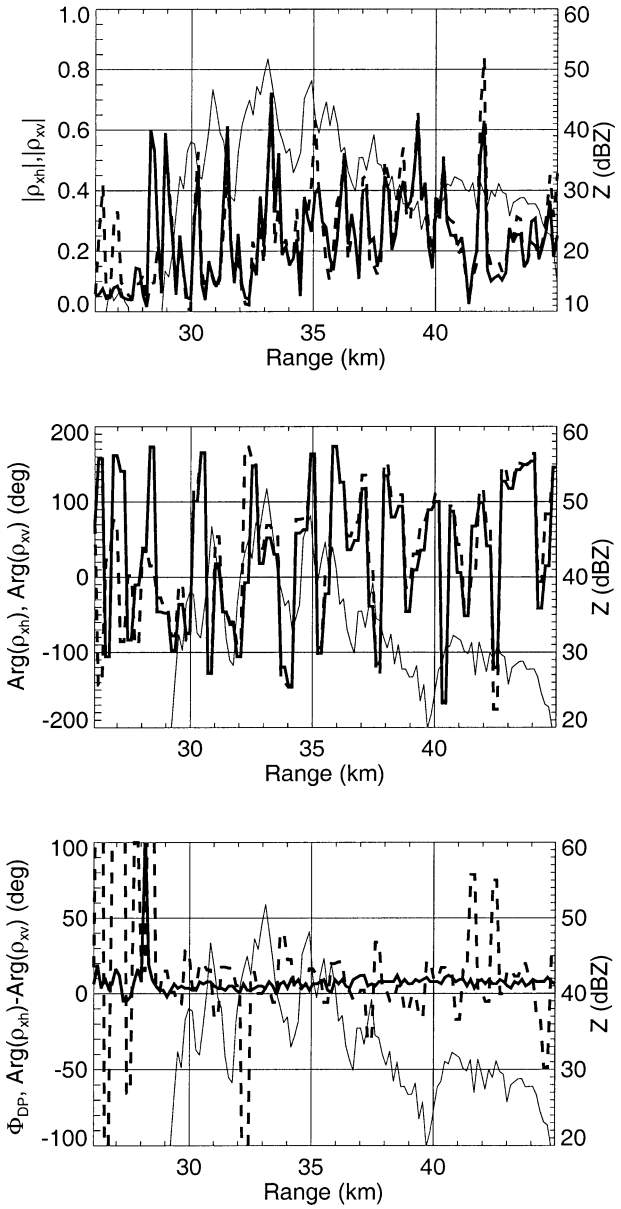

FIG. 9. Radial dependencies of nonfiltered (top) $|\rho_{xh}|$, $|\rho_{xv}|$, and Z, (middle) $\arg(\rho_{xh})$, $\arg(\rho_{xv})$, and Z, and (bottom) $\arg(\rho_{xh}) - \arg(\rho_{xv})$, Φ_{DP}, and Z for the case of 14 Aug 1998. $|\rho_{xh}|$, $\arg(\rho_{xh})$, and Φ_{DP} are shown by thick solid lines. $|\rho_{xv}|$, $\arg(\rho_{xv})$, and $\arg(\rho_{xh}) - \arg(\rho_{xv})$ are shown by thick dashed lines. Z is shown by thin solid lines. Az = 206°; El = 1.7°.

Φ_{DP} can be made in addition to the standard estimate or as its proxy, if the standard estimate is seriously compromised.

4) Both the magnitudes and the phases of ρ_{xh} and ρ_{xv} measured in rain can be effectively used for the antenna and microwave assembly quality check. Indeed, slight coupling between orthogonal channels of the dual-polarization radar (due to, e.g., feed horn misalignment, nonorthogonality of the linear polarization basis, etc.) causes an increase in the magnitude of the co-cross-polar correlation coefficients and a decrease in the magnitude of their phase fluctuations. None of the other polarimetric variables (including even LDR) is as sensitive to these artifacts.

5) The magnitude of ρ_{xh} (ρ_{xv}) combined with LDR and Z_{DR} can be used to estimate an absolute value of the mean canting angle of raindrops in the radar resolution volume according to (4), and the phase of ρ_{xh} (ρ_{xv}) gives its sign. A positive or negative trend in $|\rho_{xh}|$ ($|\rho_{xv}|$) through precipitation is an indication of nonzero net canting angle (assuming the H and V fields are properly oriented). The net canting angle in precipitation is a key issue concerning viability of the simultaneous transmission/reception scheme suggested for the upgrade of the WSR-88D radar (Doviak et al. 2000).

While it is too early to make definite conclusions regarding the range of the mean and net canting angles based on the very limited dataset, we present evidence that nonzero net canting angles θ for short propagation paths (of about 10 km) in individual convective cells with moderate-to-heavy rain do not exceed 2.5°. Preliminary examination of the full polarimetric data obtained over longer propagation paths (with Φ_{DP} exceeding 100°) during the recent field projects Tropical Rainfall Measurement Mission–Large Scale Biosphere–Atmosphere Experiment (TRMM–LBA) in Brazil and the Severe Thunderstorm Electrification and Precipitation Study (STEPS) in eastern Colorado does not reveal significant positive trends of $|\rho_{xh}|$ and $|\rho_{xv}|$ (Ryzhkov et al. 2000). Although the net canting angle θ for individual convective cells can deviate by a few degrees from zero, the average over a long propagation path along several cells is close to zero, likely because canting angles in different cells vary in sign.

It can be shown that the degree of coupling between orthogonal channels for the simultaneous transmission/reception scheme (Doviak et al. 2000) is proportional to the integral $\int \langle\alpha\rangle\Phi_{DP}\, dr$ over the propagation path. This integral is large if Φ_{DP} is large and the mean canting angle $\langle\alpha\rangle$ differs from zero and does not change its sign. The integral is quite small if a more realistic model of $\langle\alpha\rangle$ shown in Fig. 1a is assumed. Thus, judging from our preliminary analysis, we do not expect substantial coupling between orthogonal channels for the simultaneous scheme.

6) Rainfall estimation algorithms that involve specific differential phase K_{DP} and differential reflectivity Z_{DR} should be corrected if the raindrop canting angle distribution has the rms width σ exceeding about 10°. Our estimates from the two storms have dominant values of σ within 5°–10° for rain near the ground. This dispersion of the canting angles leads to a K_{DP} and Z_{DR} decrease of less than 6% compared to the case with the absence of canting. This bias is, probably, tolerable given larger uncertainties caused by the variability of drop size distributions. Nonetheless, in cases with broader canting angle distributions, raindrop canting should be accounted for when polarimetric rainfall estimation is made.

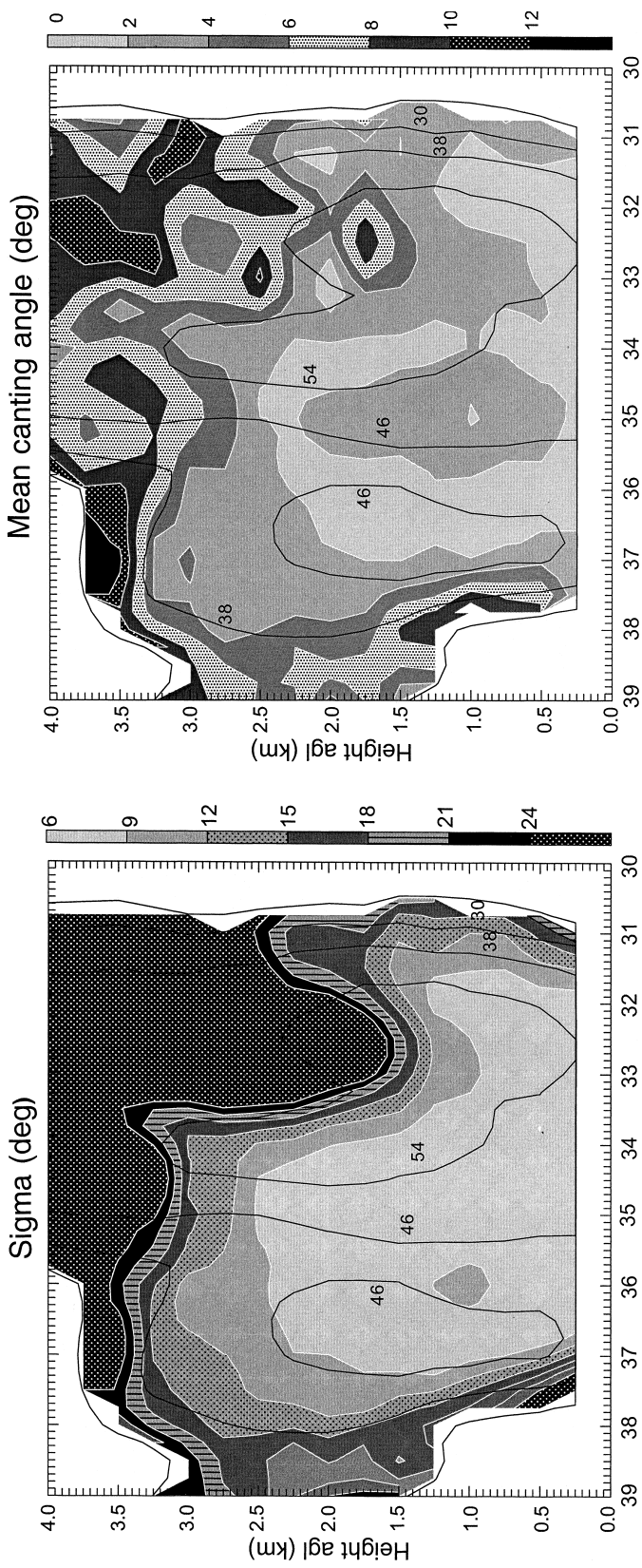

FIG. 10. RHI plots of (a) σ and (b) $|\langle\alpha\rangle|$ for the storm on 8 Aug 1998 in Colorado. Superimposed on the plots are contours of Z.

Acknowledgments. Two of the authors, V. N. Bringi and J. C. Hubbert, acknowledge support from NSF Grant ATM-9730231 and from NASA Contract NAG5-77170004. The activities of J. Vivekanandan and E. A. Brandes were supported in part by funds from the NSF that have been designated for the U.S. Weather Research Program at NCAR. E. A. Brandes was also supported by the FAA under FAA–UCAR Cooperative Agreement DTF01-98-C-00031. A. V. Ryzhkov and D. S. Zrnic appreciate Y. Liu's help in reading the S-Pol radar data.

Part of this research is in response to requirements and funding by the Federal Aviation Administration (FAA).

REFERENCES

Beard, K. V., and A. R. Jameson, 1983: Raindrop canting. *J. Atmos. Sci.,* **40,** 448–454.

Brandes, E. A., A. V. Ryzhkov, and D. S. Zrnic, 2001: An evaluation of rainfall from specific differential phase. *J. Atmos. Oceanic Technol.,* **18,** 363–375.

Brunkow, D. A., V. N. Bringi, P. C. Kennedy, S. A. Rutledge, V. Chandrasekar, E. A. Mueller, and R. K. Bowie, 2000: A description of the CSU–CHILL national radar facility. *J. Atmos. Oceanic Technol.,* **17,** 1596–1608.

Caylor, I. J., and V. Chandrasekar, 1996: Time-varying ice crystal orientation in thunderstorms observed with multiparameter radar. *IEEE Trans. Geosci. Remote Sens.,* **34,** 847–858.

Doviak, R. J., and D. S. Zrnic, 1993: *Doppler Radar and Weather Observations.* Academic Press, 562 pp.

——, V. N. Bringi, A. V. Ryzhkov, A. Zahrai, and D. S. Zrnic, 2000: Considerations for polarimetric upgrades to operational WSR-88D radars. *J. Atmos. Oceanic Technol.,* **17,** 257–278.

Hubbert, J. C., V. N. Bringi, and L. D. Carey, 1998: CSU–CHILL polarimetric measurements from a severe hailstorm in eastern Colorado. *J. Appl. Meteor.,* **37,** 749–775.

——, ——, and G. Huang, 1999: Construction and interpretation of S-band covariance matrices. Preprints, *29th Conf. on Radar Meteorology,* Montreal, Canada, Amer. Meteor. Soc., 205–207.

Jameson, A. R., M. J. Murphy, and E. P. Krider, 1996: Multiple-parameter radar observations of isolated Florida thunderstorms during the onset of electrification. *J. Appl. Meteor.,* **35,** 343–354.

Krehbiel, P., T. Chen, S. McCrary, W. Rison, G. Gray, and M. Brook, 1996: The use of dual-channel circular-polarization radar observations for remotely sensing storm electrification. *Meteor. Atmos. Phys.,* **59,** 65–82.

Lutz, J., B. Rilling, J. Wilson, T. Weckwerth, and J. Vikekanandan, 1997: S-Pol after three operational deployments, technical performances, sitting experiences, and some data examples. Preprints, *28th Conf. on Radar Meteorology,* Austin, TX, Amer. Meteor. Soc., 286–287.

McCormick, G. C., and A. Hendry, 1974: Polarization properties of transmission through precipitation over a communication link. *J. Rech. Atmos.,* **8,** 175–187.

——, and ——, 1975: Principles for radar determination of the polarization properties of precipitation. *Radio Sci.,* **10,** 421–434.

Olsen, R. L., 1981: Cross-polarization during precipitation on terrestrial links: A review. *Radio Sci.,* **16,** 761–779.

Pruppacher, H. R., and R. L. Pitter, 1971: A semi-empirical determination of the shape of cloud and rain drops. *J. Atmos. Sci.,* **28,** 86–94.

Ryzhkov, A. V., 2001: Interpretation of polarimetric radar covariance matrix for meteorological scatterers: Theoretical analysis. *J. Atmos. Oceanic Technol.,* **18,** 315–328.

——, and D. S. Zrnic, 1996a: Assessment of rainfall measurement that uses specific differential phase. *J. Appl. Meteor.,* **35,** 2080–2090.

——, and ——, 1996b: Rain in shallow and deep convection measured with a polarimetric radar. *J. Atmos. Sci.,* **53,** 2989–2995.

——, and ——, 1998: Discrimination between rain and snow with a polarimetric radar. *J. Appl. Meteor.,* **37,** 1228–1240.

——, ——, V. N. Bringi, G. Huang, E. A. Brandes, and J. Vivekanandan, 1999: Characteristics of hydrometer orientation obtained from radar polarimetric measurements in a linear polarization basis. *Proc. IGARSS'99,* Hamburg, Germany, IEEE, 702–704.

——, ——, J. C. Hubbert, V. N. Bringi, J. Vivekanandan, and E. A. Brandes, 2000: Interpretation of polarimetric radar covariance matrix for meteorological scatterers. *Proc. IGARSS'2000,* Honolulu, HI, IEEE, 1584–1586.